Production and Evaluation of Heavy-Section Ductile Cast Iron

H. Itofuji
K. Kawamura
N. Hashimoto
H. Yamada
Ube Steel Co., Ltd.
Ube City, JAPAN

ABSTRACT

Ferritic ductile cast iron with a weight of 36 ton and a maximum wall thickness of 245 mm was produced with no riser under the controlled cooling method. The important places of the casting were evaluated on the microstructure, defects, and mechanical properties, such as tensile strength, CVN impact value, rotating bending fatigue, fracture toughness, and crack sensitivity.

The solidification time was reduced 80% at the heaviest section to get a good spheroidal graphite morphology by chillers. The cast designing was simulated by computer and the result showed good matching with the practice. The mold movement was measured not only between lower and upper mold, but also around the lower mold during the solidification to confirm the mold rigidity and clamping. No shrinkage was observed in the casting when it was evaluated by ultrasonic testing.

The results of mechanical properties were almost homogeneous among the evaluated parts and were quite satisfactory as ferritic ductile cast iron with heavy section.

Table 1.
Chemical Composition of Raw Materials

Row Material	Chemical Composition (Wt%)							
	C	Si	Mn	P	S	Ca	Al	Bl
Pig iron	4.17	0.26	0.03	0.027	0.015	tr.	tr.	Fe
Steel scrap	0.01	1.11	0.19	0.011	0.008	tr.	tr.	Fe
Fe-Si	0.05	75.7	tr.	0.015	0.005	0.34	1.27	Fe
Sic	60.6	26.4	-	-	0.070	-	0.2	Ash
Carbon	99.0	-	-	-	0.020	-	-	Ash
Graphite	60.0	-	-	-	tr.	-	-	Ash

INTRODUCTION

Recently, the demand for heavy-duty ductile cast iron has been increasing all over the world, and the required quality has become more demanding. To produce heavy-duty, heavy-section ductile cast iron and obtain a better reliability from the user, many papers on practical data have been checked and discussed in our foundry. Even the solidification mechanism of ductile cast iron has been studied[1-3] to improve the quality.

It has been generally said that the production of heavy-section ductile cast iron was rather more difficult than a small-section one because of the longer solidification time. This long solidification brings some problems to the casting, such as the degeneration of nodule size and shape, chunky graphite precipitation, carbide precipitation, microshrinkage, etc. The chunky graphite precipitation has been the biggest problem. Therefore, countermeasures have been studied for many years.[4-25] Many researchers[4-12] have reported that the most effective method was to reduce the solidification time by using chillers, although there are some other methods[13-25] to avoid chunky graphite. In our foundry, several countermeasures were discussed and standardized considering the following solidification mechanism:[1-3]

1) *Chemical composition (Wt %);* 3.40–3.50C, 2.10–2.40Si, <0.35Mn, <0.050P, <0.010S, <0.0050Ca, <0.005Ce, 0.040–0.055Mg, 4.20–4.30CE, and <0.20 other impurities.
2) *Casting design;* riserless casting and solidification control.
3) *Mold;* furan-bonded sand and rigid clamping.
4) *Melt treatment;* use low Al-, Ca-, Ce-, and Sr-contained spheroidizer and inoculant; and avoid a large addition of Si .
5) *Pouring;* pour at 1310±10C shortly after melt treatment.

In this paper, the result of producing and evaluating ferritic heavy-section ductile cast iron will be introduced. The casting was part of a 2800-ton plastic injection machine. The evaluation was done on the soundness and the mechanical properties.

PRODUCTION AND EVALUATION PROCEDURE

Melting and Treatment

The nominal capacity of our arc furnace is 30 ton, but we can melt the metal up to 45 ton. Forty-ton melts were prepared by a 30-ton arc furnace with a magnesia lining. The composition of raw materials is shown in Table 1. After the melts reached 1520C, they were slagged off and tapped into a ladle at 1500C. The main composition, such as C and Si, was adjusted under pure argon bubbling from the bottom of the ladle. The melt was moved to a nearby mold, then poured into another ladle and treated with spheroidizer and inoculant at 1400C. The treatment condition is shown in Table 2.

Table 2.
Treatment Condition of Melt

Row Material	Chemical Composition (Wt%)							Addition			Reaction Time
	Si	Ba	RE	Ca	Mg	Al	Bl	Wt%	Method	Temperature °C	Min
Spheroidizer	45.90	-	0.39	2.04	5.86	0.33	Fe	1.2	Sand witch	1400	≒ 3
Incoulant	73.53	1.40	-	2.45	-	1.72	Fe	0.3			

Casting Design

The casting produced and evaluated in this study is shown in Figure 1. It had been considered that a shrinkage-free casting with no riser would be possible and the solidification time should be controlled within 200 minutes[8] to obtain good nodularity and satisfactory mechanical properties. For these reasons, a computer simulation system was introduced. The solidification time and shrinkage were controlled using the chillers made from ductile cast iron.

The chillers were designed by computer simulation. The explicit finite difference method was used for the simulation. The basic data for simulation is shown in Table 3. As the result of the simulation, the solidification time was scheduled 150 minutes at the heaviest section. Since many chillers were put on the parting line between an upper and lower mold, a fast cooled solid shell was also expected to enclose the eutectic expansion as a rid. (The term "rid" will be explained later.) The chiller design is shown in Figure 1. The gating system was based on Figure 2[35] and the following formula:

$$A_s : A_r : A_c = 1 : 2 : 0.72 \quad (1)$$

where

A_s = Cross sectional area of sprue

A_r = Cross sectional area of runner

A_c = total cross sectional area of choke

Molding

Furan-bonded sand was used as the rigid mold material. Flask was 4000-mm W x 4000-mm D x 3100-mm high. The upper and lower mold were rigidly clamped by eight steel bars of 75-mm dia. The mold was dried at 130C for 12 hours.

Pouring

The melt was poured into the mold at 1320C through a pouring basin, which took about 120 seconds. The solidification time was measured at the heaviest wall thickness to check the matching with the results of the computer simulation. The mold movement was also optically measured at three points on the upper mold and four points around the lower mold to check the mold and clamp rigidity during the eutectic expansion.

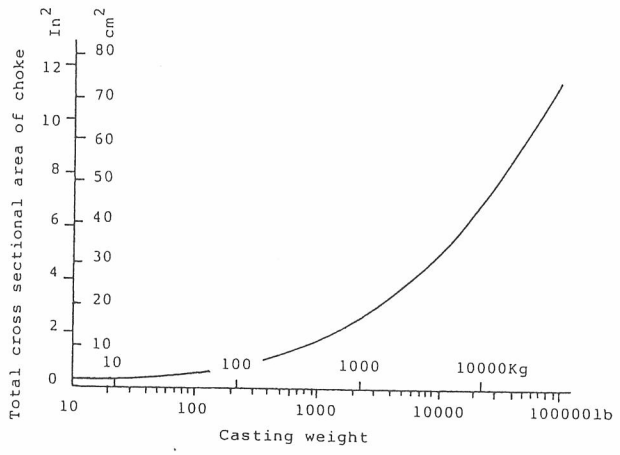

Fig. 2. Selection guide for total cross-sectional area of choke.[35]

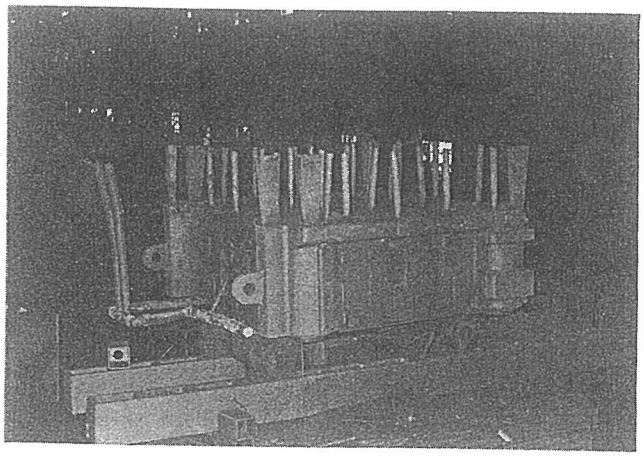

(1a)

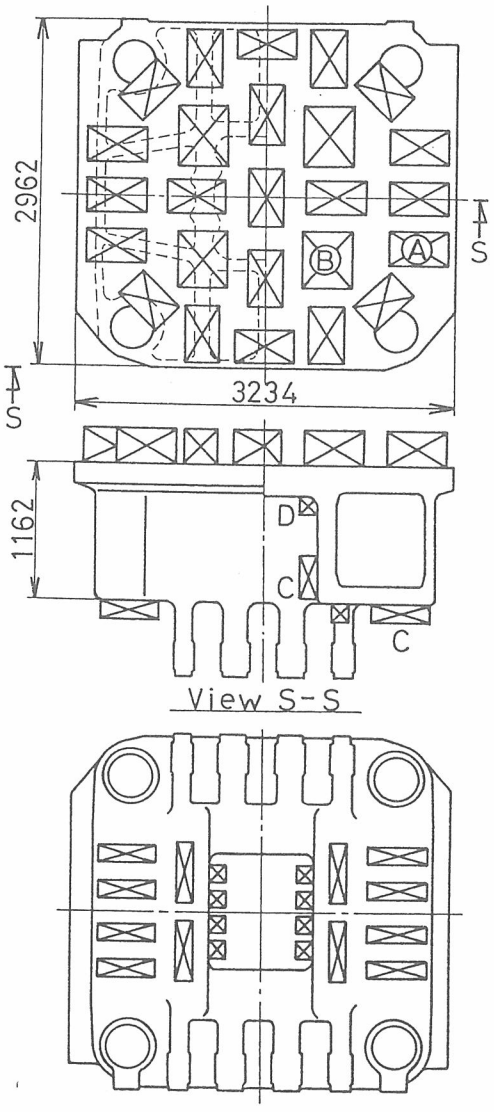

(1b)

Fig. 1. As-cast appearance (a) and chiller design (b) of ductile cast iron studied in this work; max. wall thickness = 245 mm, rough weight = 36 ton. Chiller A = 300x300x500 mm, B = 400x400x500 mm, C = 150x150x500 mm, D = 150x150x150(R150) mm.

Table 3.
Basic Data for Computer Solidification Simulation

Material	Thermal conductivity Cal/cm^2·sec·°C	Density g/cm^3	Specific heat Cal/g·°C	Latent heat Cal/g	Initial Temp °C	Liquidus Temp °C	Solidus Temp °C	Solid ratio %
Ductile cast iron	0.06	6.90	0.20	50.0	1250	1170	1130	75.0
Chiller	0.08	7.60	0.16	-	20.0	-	-	-
Silica sand	0.003	1.60	2.50	-	20.0	-	-	-
Air	-	-	-	-	20.0	-	-	-

Knock-Out and Heat Treatment

After the casting reached about 550C, it was knocked out from the mold, followed by stress relief treatment at 560C for 8 hours.

Evaluation of Casting

The soundness at critical sections of the casting (Fig. 3) was evaluated by ultrasonic testing. Because the chillers were used on them, the nodularity would be good; therefore, it was quite easy to check. The mechanical properties at room temperature were also evaluated at the hatched parts in Figure 3. The test procedure is shown in Table 4.

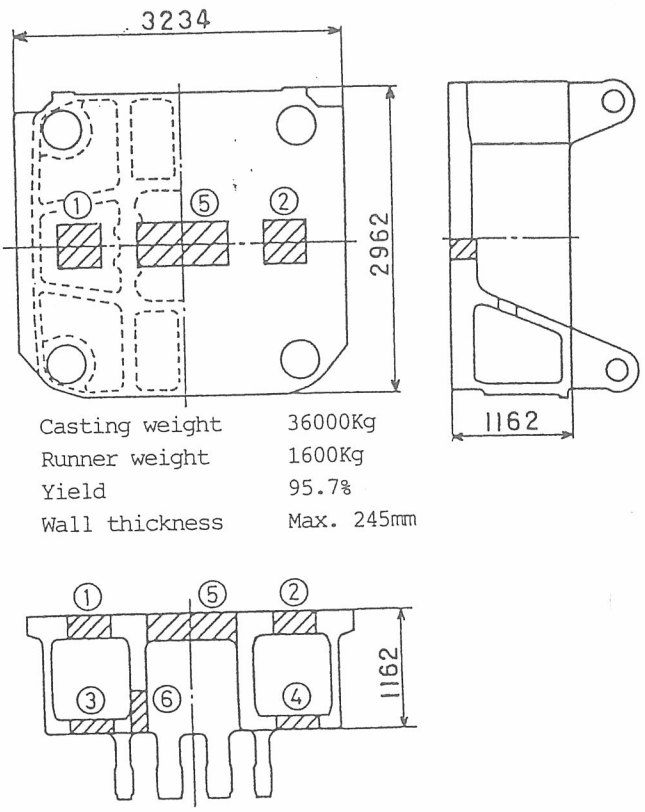

Fig. 3. Important parts on structure designing as casting (hatched portions).

RESULTS

Chemical Composition

The main chemical composition of the melt at pouring basin was analyzed with a Quantmeter. The impurities and gas elements were analyzed with an inductively-coupled vacuum plasma spectrometer and gas analyzer for each. The results are shown in Table 5. This is the typical chemical composition for heavy-section ductile cast iron in our foundry.

Solidification Time

The simulated and measured results on the solidification process are shown in Figure 4. Thermocouples were set below the center of the wall thickness, about three-fourths from the top surface, as shown in Figure 4. This was the reason the hot spots were predicted there by the computer simulation. The results showed that there was a good matching between the simulation and measurement, and it took about 140 minutes at the heaviest section. If the solidification was not controlled, it would take about 12 hours according to the same simulation. It meant that the solidification time was reduced about 80 percent.

Mold Wall Movement

The results of the mold wall movement at several points of the mold are shown in Figure 5a. As the comparative data, the mold wall movement by a conventional casting design is shown in Figure 5b. Points 1, 2, 3, and 4 in Figure 5 were places where the mold wall movement was measured at the side wall of the lower mold. The other points were places where the mold wall movement was measured between the upper and lower mold.

Table 4.
Test Procedure for Each Mechanical Property

Test	Specimen	Term	Tested part
Tensile properties	14mm diameter bar 50mm gauge length	Strain speed ; 3.3×10^{-4} 1/sec	(2) (4) (5) (6)
Impact value	2mm V-notch 10mm square bar	Impact enargy ; 3Kgf·m Room temp.	(2) (4) (5) (6)
Brinell hardness	Holder of tensile specimen	10mm/3000Kg	(2) (4) (5) (6)
Rotating bending fatigue	12mm diameter bar	Rotating speed ; 3000rpm Max. moment ; 1.5Kg·m	(1) (3) (5)
Elastic-plastic fracture tuoghness J1c	1"TCT ; 25.4mm thickness by ASTM E813	Unloading compliance method	(5)
Crack sensitivity ΔKth	5"TCT ; 25.4mm thickness by ASTM E647-78T	Direct method	(5)

Table 5.
Chemical Composition of Melt at Pouring Basin

Chemical composition (Wt%)

C	Si	Mn	P	S	Ca	Ce	Mg	CE	OI	O (ppm)	N
3.46	2.36	0.28	0.045	0.007	0.0024	0.004	0.043	4.25	0.16	3.0	61.0

CE = T·C+1/3
OI = Other impurities
= Cr+Ti+Sn+Al+As+Pb+Sb+Bi+Zn+V+Nb

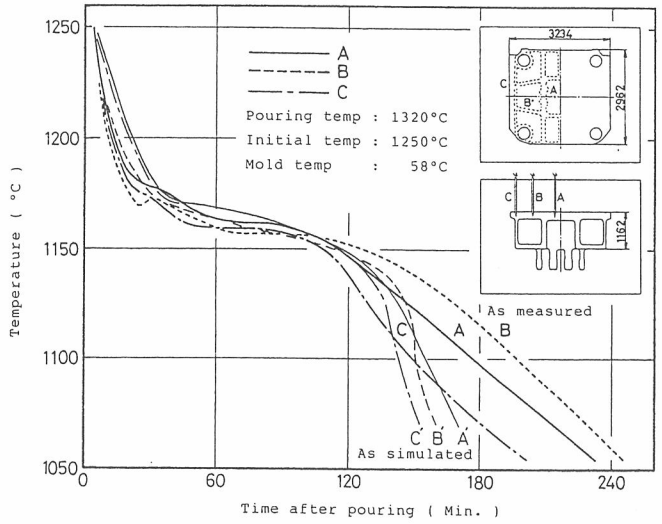

Fig. 4. Real and simulated cooling curve at heaviest section in casting.

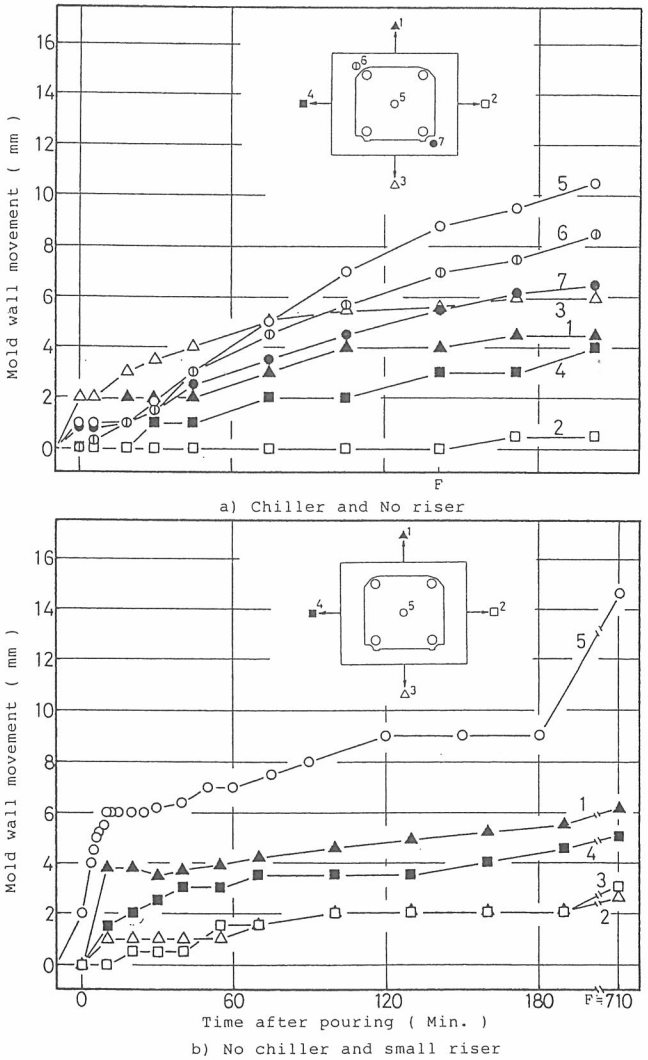

Fig. 5. Mold wall movement between upper and lower mold (>position 5) and around lower mold (positions 1–4) after pouring, under same condition except riser and chiller design. F = finish time of eutectic solidification.

observed to be about 9 mm in this controlled casting design until the solidification was completed. On the other hand, the mold wall movement around the side wall of the lower mold was 0.5–5.5 mm during the same period. However, some of them might not be a real expansion of the casting at each point, because there would be some expansion of the sand mold and chillers. Actually, most of the measured points were continuously moved, even after the eutectic solidification was completed. It seemed that the weakest side around the lower mold wall concentrically received the expansion force. The chiller effect on the mold wall movement was compared with point 5 in Figures 5a and 5b. There was quite a small movement in Figure 5a, but a big movement in Figure 5b just after pouring. This means that a buoyancy from the melt before the solidification, and a eutectic expansion force during the solidification, toward the upper mold, could be reduced by the chilled, thicker solid shell. This was named the "rid" effect of chiller after this work. It is considered that the effect is quite helpful for the riserless castings, because the eutectic expansion can be used rather effectively to compensate the liquid and solid shrinkage during the solidification.

Soundness

Figure 1 shows the as-cast appearance of the casting just after the shot blast. There was no visible surface shrinkage or swelling at all. Good appearance was obtained.

As the result of ultrasonic testing, shrinkage larger than a diameter of 6.3 mm was not observed at the important parts of the casting at all. This meant that no macroshrinkage was observed in the casting, because, if the shrinkage occurred, it would be porous and be more than 6.3 mm. Quite a good echo was observed at all the important parts. An example of the echo is shown in Figure 6. Actually, no visible shrinkage was observed at the section of each test block taken from casting for the evaluation.

Tensile Properties

The results are shown in Table 6; the superior result occurring as heavy section was obtained. Especially, 0.2% proof stress and tensile strength were almost homogeneous among every selected part in the casting. Although elongation and reduction in area were scattered within about 10%, the lowest value was approximately 15% for each. These values were not too bad. The tendency was for the chiller side to be the best and the opposite side to be the worst.

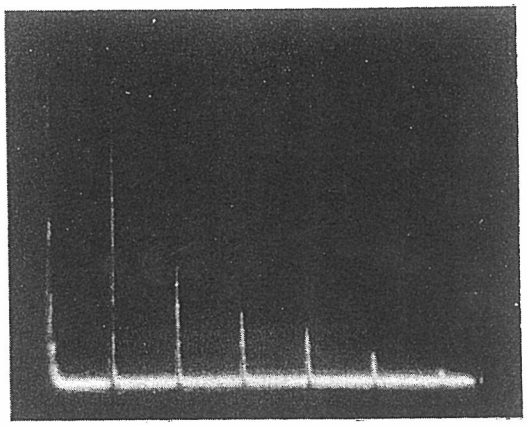

Fig. 6. Echo observed by ultrasonic test at heavy section in casting.

was caused by nodule shape, size, and spacing, as mentioned by many researchers.[26–28] A representative microstructure and the result of the microstructural analysis at position 5 are shown in Figure 7 and Table 7. The good nodularity and high ferrite ratio was obtained at all the evaluated parts.

It is generally said that high Mn content reduces the ductility in heavy sections because of Mn segregation and a carbide precipitation. But, if the solidification time was reduced for such a heavy section, the Mn segregation would be weaker and the high ferrite ratio would be obtained. Tensile strength, elongation and reduction in area were extremely reduced when Mg dross occurred. Then, 0.2% proof stress was slightly reduced.

Brinell Hardness

The results are shown in Table 6. No difference was observed among the parts in the casting.

Charpy V-Notch Impact Value

The results are shown in Table 6. The chiller side showed the best result. The Mg dross layer at position 5 was also evaluated and showed a good value. It was considered that the evaluated layer was close to the chiller surface, and that the v-notch was machined parallel against the surface and the dross direction. Therefore, dross did not decline the value. A good ferrite ratio and nodularity and their size also offered the better value.

Rotating Bending Fatigue

The test was done at positions 1, 3, and 5 as representative sections in the casting. Since the surface layer was important for stress fatigue strength, the specimens for rotating bending fatigue test were taken out from each surface layer.

The surface of 15 mm was machined off at positions 1 and 5. Then the specimen was taken out of the machined surface layer because of the dross layer. It was considered that the casting was a symmetrical object and that the mechanical properties were the same as the symmetrical part. Therefore, tensile strength of surface layer at positions 2 and 4 were used for the calculation of endurance ratio at positions 1 and 3 for each. The results are shown in Figure 8. Stress ratio, R, and endurance ratio, ER, were calculated by following fomulas:

$$R = \text{Min. stress} / \text{Max. stress} \quad (2)$$

$$ER = \text{Fatigue limit} / \text{Tensile strength} \quad (3)$$

Here, satisfactory fatigue limit and endurance ratio as heavy section were also obtained. Palmer et al.[29] have reported that the endurance ratio of ferritic ductile cast iron was reduced when the wall thickness increased and it was around 0.42 for 304-mm dia. test block. However, the results at all positions in this study were higher than this value, especially positions 1 and 5, although the mass was much bigger than their test block. This might be the result of the solidification control. This meant that a good nodularity and smaller graphite nodule brought good tensile properties, fatigue limit, and endurance ratio. Many researchers have mentioned this in their papers.[30,31] It was a tendency that a scattering of fatigue life at each stress became bigger when the wall thickness increased.

Result of Tensile, Hardness, and Impact Test on Casting

Part		$PS_{0.2}$	TS	El	RA	HB	CVN
(2) 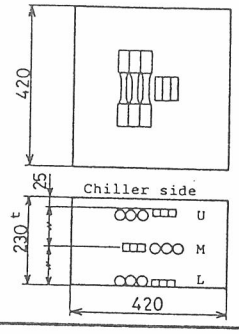	U	25.6	38.9	27.3	23.6	144	1.5
		25.3	38.3	24.6	21.3	146	1.6
		25.5	39.3	24.6	23.2	147	1.5
	M	25.7	39.5	20.3	18.1	143	1.0
		25.9	39.6	21.0	19.1	140	0.9
		25.6	39.5	21.6	19.4	140	0.8
	L	25.9	38.7	21.0	16.9	137	1.0
		26.0	38.0	21.4	18.8	143	1.1
		26.1	38.8	21.7	20.7	146	1.0
(4) 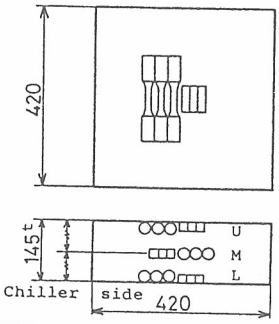	U	26.3	38.9	16.4	15.4	147	1.0
		26.0	39.2	22.4	20.6	138	0.9
		26.2	38.7	14.8	17.4	137	1.0
	M	26.2	39.7	20.6	17.2	140	0.9
		26.1	39.6	18.4	15.9	141	0.9
		26.0	39.2	16.0	12.1	143	0.8
	L	26.1	39.9	25.6	24.1	147	1.4
		26.4	39.9	21.2	22.3	146	1.5
		26.3	39.9	24.6	23.2	143	1.4
(5) 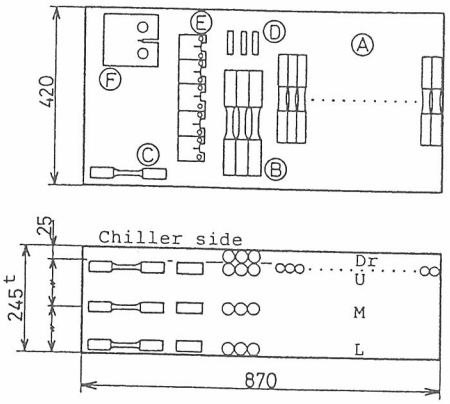	Dr	24.7	32.8	6.0	8.4	137	1.5
		25.3	33.1	6.0	11.1	146	1.4
		25.3	33.5	4.2	9.8	143	1.5
	U	26.0	39.6	24.8	24.1	143	1.3
		26.3	40.0	25.0	24.1	143	1.3
		26.3	39.6	24.0	22.8	140	1.3
	M	26.3	39.6	16.0	13.8	140	0.9
		26.3	39.6	17.0	16.4	140	0.9
		26.6	40.0	19.6	17.7	143	1.0
	L	26.6	39.3	21.4	20.3	140	1.1
		27.0	39.0	19.0	19.0	143	1.0
		27.0	38.7	16.6	16.4	140	1.0
(6) 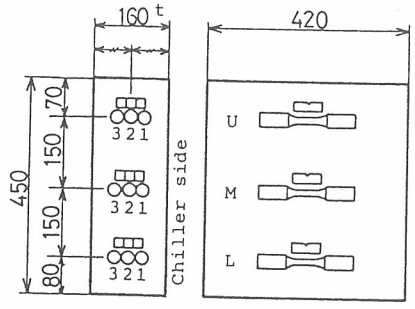	1	25.6	39.1	23.6	18.8	140	1.4
	U2	25.8	39.2	23.0	17.9	146	1.1
	3	26.1	38.9	16.8	14.7	140	1.0
	1	25.9	39.5	29.2	25.7	142	1.1
	M2	25.2	39.4	22.8	19.3	147	1.3
	3	25.3	39.1	18.0	16.8	143	0.9
	1	25.7	39.3	25.6	23.5	135	1.1
	L2	25.6	39.2	16.2	17.3	140	1.1
	3	25.9	39.2	19.6	17.6	139	1.1

Nomenclature

$PS_{0.2}$; 0.2% proof stress(Kgf/mm^2)
TS ; Tensile strength(Kgf/mm^2)
El ; Elongation(%)
RA ; Reduction of area(%)
HB ; Brinell hardness(10/3000)
CVN ; Charpy V-notch impact value(Kgf·m/cm^2)
Dr ; Dross layer in wall thickness
U ; Upper layer of wall thickness
M ; Middle layer of wall thickness
L ; Lower layer of wall thickness

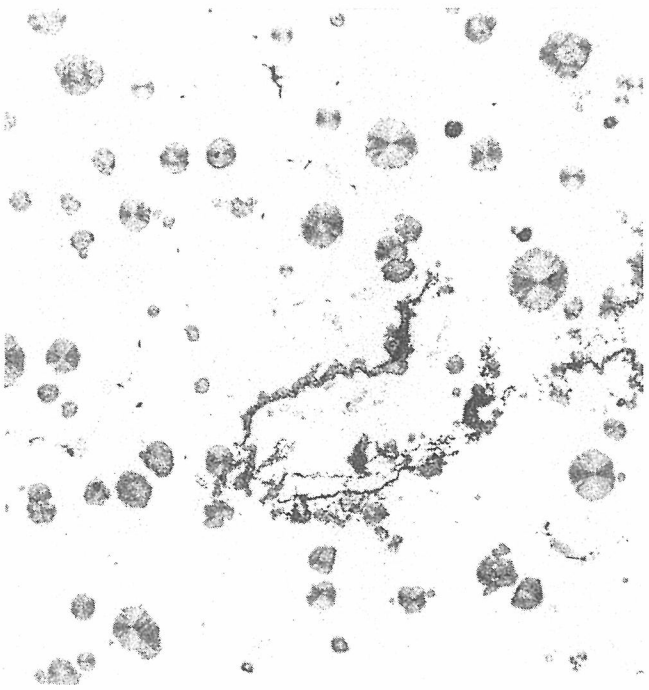

(7a) Dross layer and chiller side

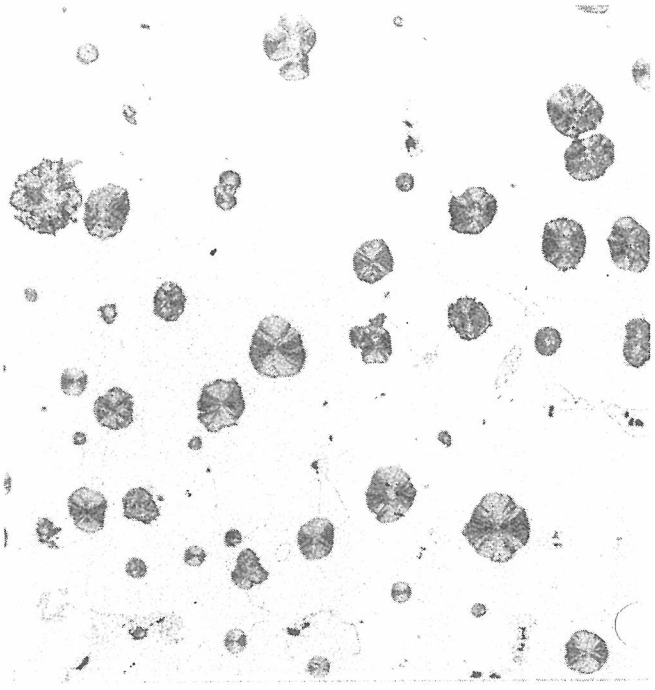

(7b) Upper layer

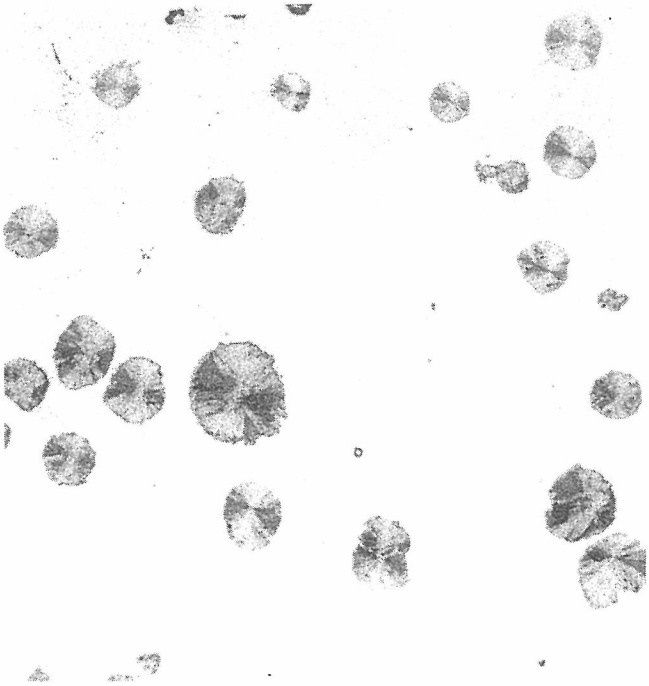

(7c) Middle layer

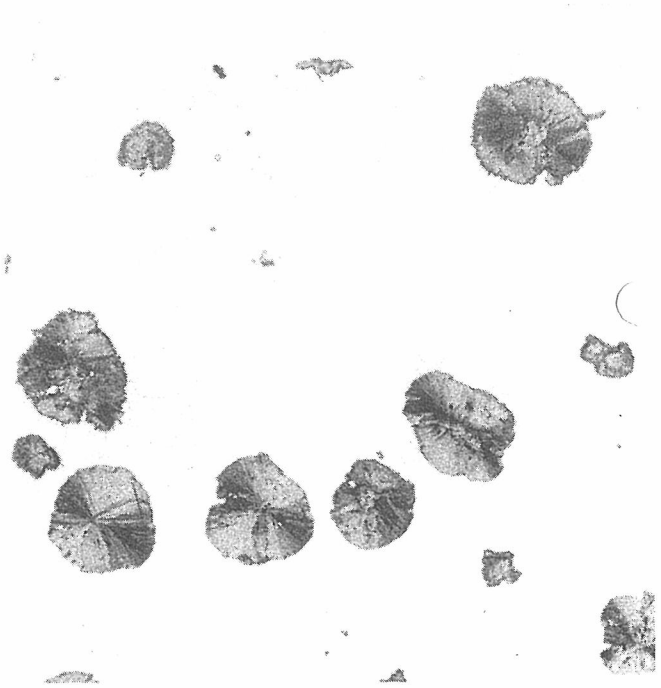

(7d) Lower layer and sand side.

Fig. 7. Microstructure at position 5 in casting. Wall thickness = 245 mm. Etched 2% Nital. 100X.

Elastic-Plastic Fracture Toughness

Since tensile properties, impact value, and fatigue limit were satisfactory at each position, an elastic-plastic fracture toughness test was done at position 5 as the representative heavy section in the casting.

The places where the specimens were taken are shown in Figure 9. To estimate K_{Ic} value from J_{Ic}, Young's modulus was measured near J_{Ic} specimen for each tested layer. There were no differences among them and the average was E=17100 Kgf/mm^2. Equation 4 was used for the calculation. Test data is shown in Figure 10, for example, and the fracture surface is shown in Figure 11.

$$K_{Ic} = (E \cdot J_{Ic} / 1 - R^2)^{1/2} \quad (4)$$

where

R = Const. = 0.3

E = 17100 Kgf/mm^2

A good R-curve was obtained for each test. The whole result is shown in Table 8. The calculated K_{Ic} value is also shown in Table 8. Although the nodule and ferrite size were different among the layers as shown in Table 7, the J_{Ic} value did not scatter among the layers, or in the layer, and was satisfactory. This was also obtained from the calculated K_{Ic} value. It was considered that the J_{Ic} value was not changed with such a small difference in graphite nodule and ferrite size, like the tensile properties, but that the high nodularity was effective for the J_{Ic} value. Kuribayashi et al.[32] have mentioned in a similar report that the J_{Ic} value was linearly increased when the nodularity was increased.

Fatigue Crack Growth Rate

The test was also done at chilled layer and opposite layer at position 5. The results is shown in Figure 12. One of the fracture surfaces is shown in Figure 13. Bhandhubanyong[33] has reported that ΔKth became larger when the solidification was slower and the nodule spacing was greater. In this study, ΔKth of the chilled side, with narrower nodule spacing, was slightly higher than that of the opposite side, but totally, the fatigue crack growth behavior was almost the same between the two layers. The ΔKth at the chilled layer was abut 28.9 Kgf/mm$^{3/2}$ and the opposite sand side layer was about 25.4 Kgf/mm$^{3/2}$.

CONCLUSION

It is considered that the heaviest-duty ductile cast irons with heavy section in recent years have been used for the containers for radioactive materials. The castings have a wall thickness of 350–500 mm and a weight of 60–100 ton. It seems that this kind of cast iron required the high quality and has already achieved it.

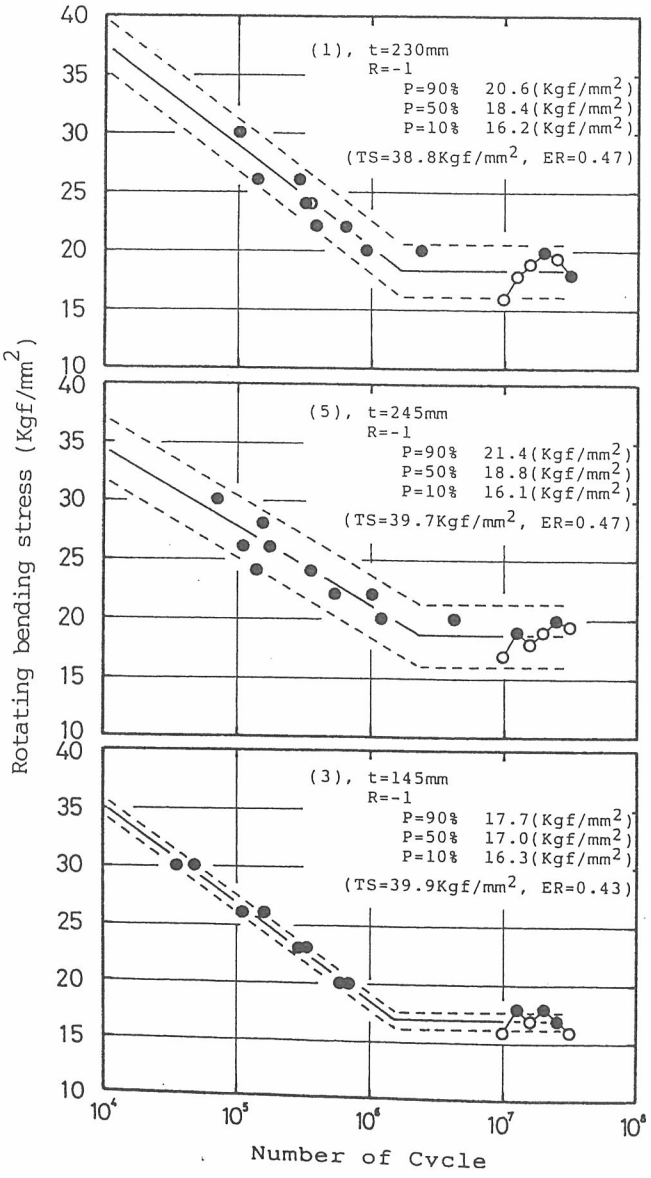

Fig. 8. S–N curve at positions 1, 3, and 5 in casting.

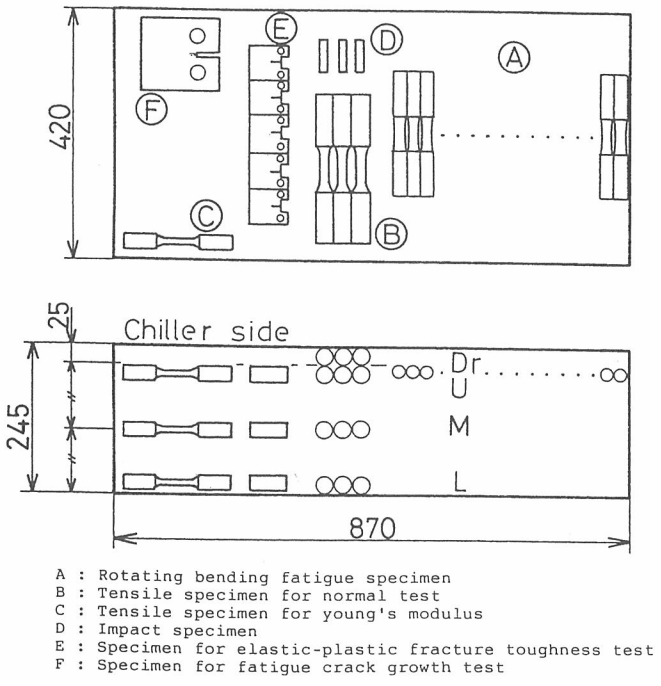

Fig. 9. Sampling place for elastic-plastic fracture toughness and crack growth rate at position 5 in casting.

The recent tendency of the mechanical properties at the thermal center of heavy section on the containers is shown in Table 9.[26-28,34] To get high impact value, Si content is reduced in these cases, such as 1.8–2.0% Si. Therefore, 0.2% proof stress and tensile strength are lower than common values. Including these properties, the containers are designed and produced. It was found that the quality of the casting in this study was already achieved to be equal to the above heavy-duty containers, besides Si adjustment and its effect.

SUMMARY

The production technology of heavy-section ductile cast iron has been established through the recognition of the relationship among the solidification mechanism, chemical composition, casting design, wall thickness, solidification control, microstructure, and mechanical properties. It was considered that, although there were some important points on the production process to get the high quality of ferritic ductile cast iron with heavy section, the most important point was to control the graphite morphology such as the nodule diameter, nodularity, and nodule spacing and, therefore, the solidification time should be severely controlled. Naturally, the ferrite shape and grain size as the matrix structure are very important for getting the superior mechanical properties. However, the good ferrite matrix structure will come from the result of the graphite nodule control.

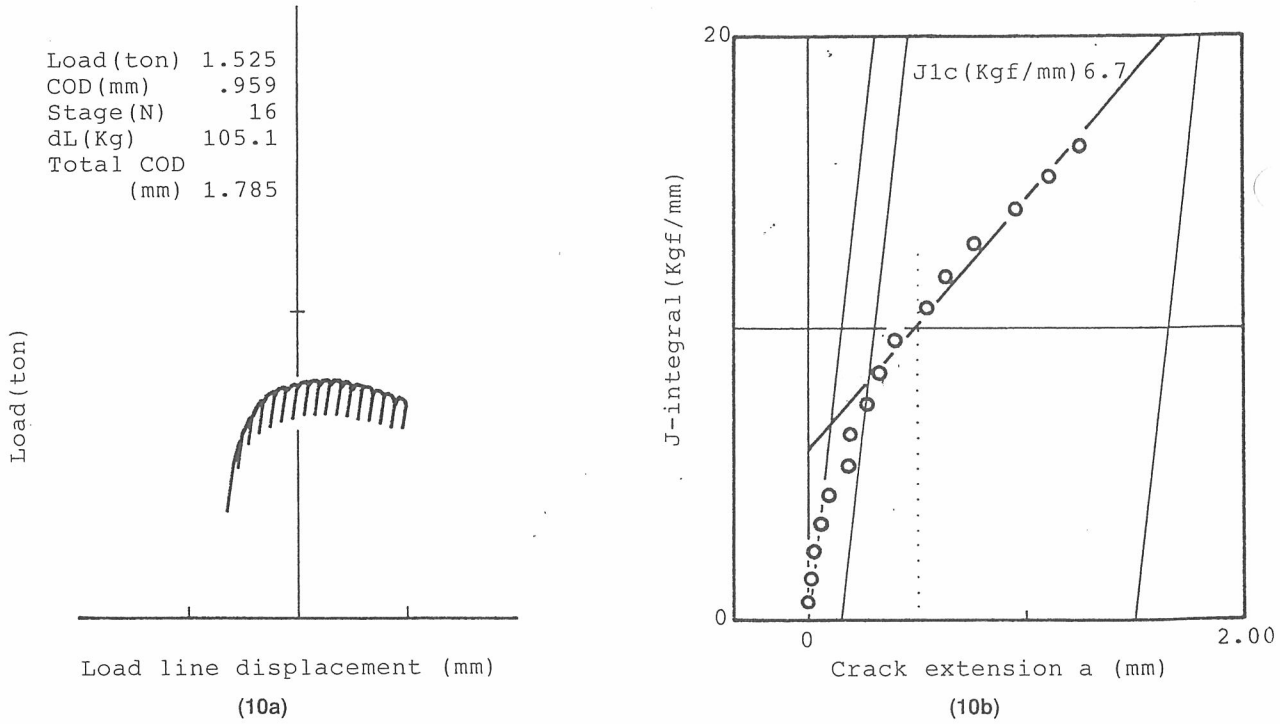

Fig. 10. Example of elastic-plastic fracture toughness data at position 5 in casting: a) load vs. load line displacement; b) J-integral vs. crack extension a.

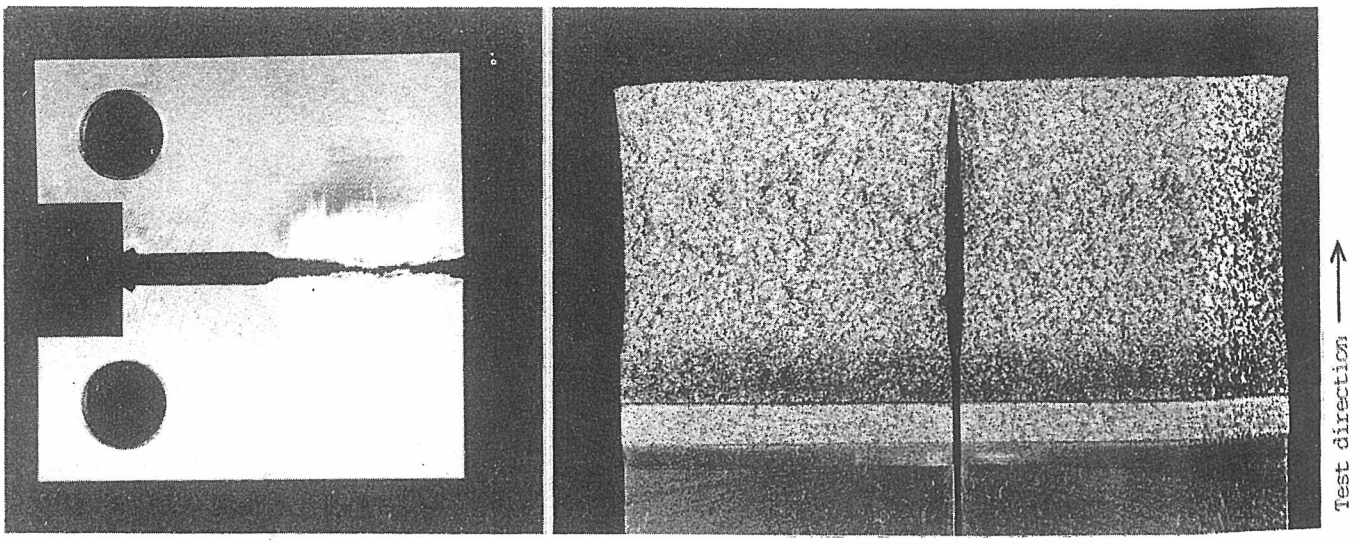

Fig. 11. Fracture surface of 1-in. CT specimen for elastic-plastic fracture toughness test; lower layer at position 5.

Table 7.
J_{Ic} and Calculated K_{Ic} Value at Position 5 in Casting

Layer	Graphite				Ferrite	
	Nodulerity (%)	Nodule diameter (μm)	Nodule spacing (μm)	Nodule number ($N/100\mu m^2$)	Area (%)	Size (μm)
Dross (Chiller side)	95	35	105	70	> 95	35
Upper	94	50	140	50	> 95	50
Middle	95	70	190	30	> 90	80
Lower (Sand side)	93	110	250	15	> 95	100

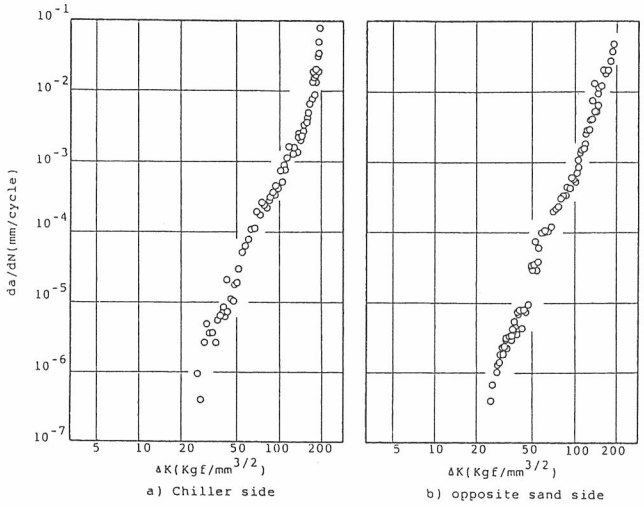

Fig. 12. Fracture crack growth rate da/dN as a function of stress intensity fracture range ΔK for wall thickness of 245 mm in ferritic ductile cast iron; position 5 in casting.

Table 8.
Result of Microstructural Analysis at Position 5 in Casting

Layer	J1c Kgf/mm	K1c $Kgf/mm^{2/3}$
Upper	5.9	333
	5.8	330
	6.8	357
	Ave.6.2	Ave.340
Middle	4.6	294
	6.3	344
	5.2	313
	Ave.5.4	Ave.317
Lower	5.6	321
	6.7	355
	7.0	363
	Ave.6.4	Ave.346

Table 9.
Recent Tendency of Mechanical Properties on Heavy-Duty Ductile Cast Iron with Heavy Section (Wall thickness 350–500 mm, weight 60–100 ton)

Tensile properties[34]				Brinell[34] hardness	Impact[34] value, CVN	Fracture Toughness	
0.2% Proof Stress (Kgf/mm^2)	Tensile Strength (Kgf/mm^2)	Elongation (%)	Reduction in area (%)	(10/3000)	($Kgfm/cm^2$)	K_{Ic}[26] ($Kgf/mm^{3/2}$)	J_{Ic}[28] (Kgf/mm)
≒21.2	35.8-36.8	15.0-20.9	15.1-25.3	126-130	2.8-2.9	230-330	3.2-4.4

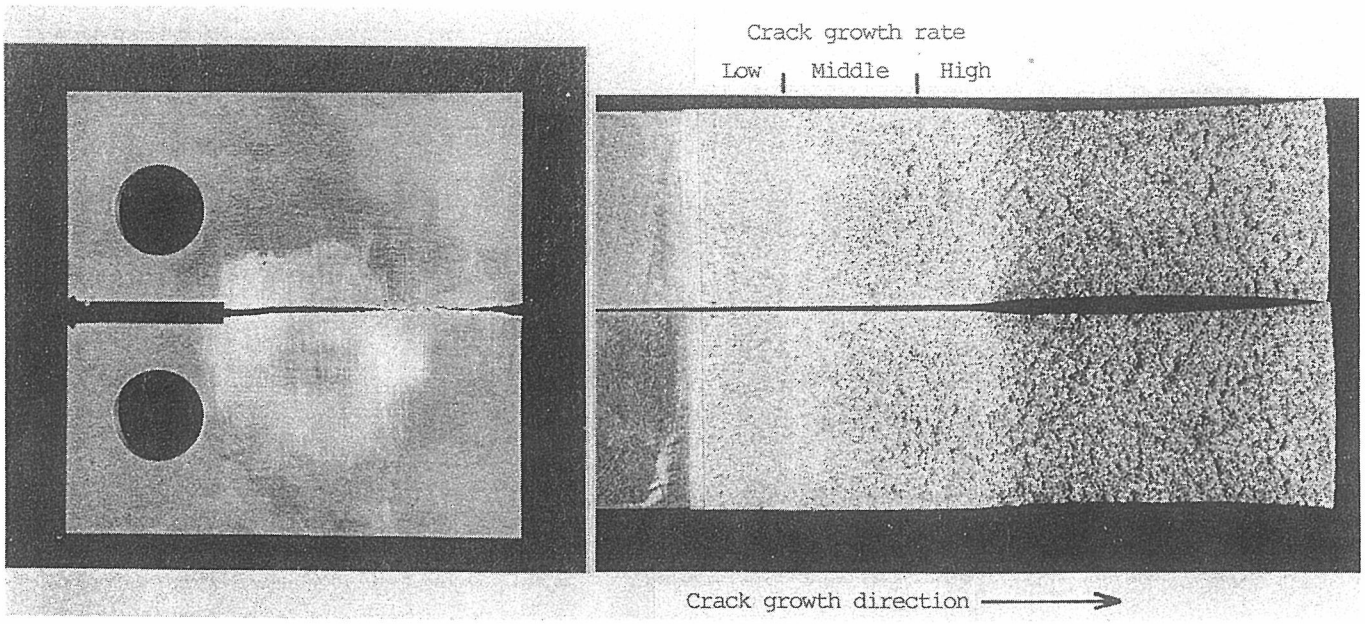

Fig. 13. Fracture surface of 1-in. 5TCT specimen for fatigue crack growth rate test; chiller side at position 5 in casting.

ACKNOWLEDGMENT

The authors would like to acknowledge Dr. H. Shingu and Dr. N. Inoyama of Kyoto University for their comments in assembling this manuscript.

REFERENCES

1. H. Itofuji, Y. Kawano, S. Yamamoto, N. Inoyama, H. Yosida, and B. Chang; "Comparison of Substructure of Compacted/Vermicular Graphite with Other Types of Graphite; "AFS *Transactions*, vol 91, p 313 (1983).
2. H. Itofuji, Y. Kawano, N. Inoyama, S. Yamamoto, B. Chang, and T. Nishi; "The Formation Mechanism of Compacted/Vermicular Graphite in Cast Iron," *AFS Transactions*, vol 91, p 831 (1983).
3. H. Itofuji and H. Uchikawa; "Formation Mechanism of Chunky Graphite in Heavy-section Ductile Cast Irons," The 94th AFS Congress paper to be presented (1990).
4. R. K. Buhr; "Vermiculite Graphite Formation in Heavy-Section Nodular Iron Castings" *AFS Transactions*, vol 76, p 497 (1968).
5. R. R. Kust and C. R. Loper, Jr.; "The Production of Heavy-Section Ductile Iron," *AFS Transaction*, vol 76, p 540 (1968).
6. T. W. Parks, Jr., N. G. Berry, and C. R. Loper, Jr.; "The Effect of Solidification Time and Section Size on the Mechanical Properties and Microstructure of High-Carbon Ferrous Alloys," *AFS Transactions*, vol 76, p 565 (1968).
7. H. Mayer; "Heavy-Section Castings in Ductile Iron," *AFS International Cast Metals Journal*, (Dec 1976).
8. Y. Maebashi and S. Arimoto; *Improvement of Ductile Cast Iron*, p 303 (1982).
9. A. Munichi; "160t Pressenstander," *Konstruieren und gießen 9*, Nr. 1, p 4 (1984).
10. M. Sappok, Seminar "Containers for Radioactive Materials Made from Nodular Cast Iron," in Berlin, p 215 (June 9–10, 1987).
11. H. Lindscheid and D. Schock; "Verfahren zur Steuerung der Erstarrungs und Abkuhlungsbedingungen fur Gußstucke aus Gußeisen," *Giesserei*, vol 75, Nr. 22, p 674 (1988).
12. O. Liesenberg and P. Wolf; "Effect of Chillers on Ductile and Gray Iron," *Foundry Trade Journal*, vol 163, p 292 (1988).
13. R. K. Buhr; "The Effects of Pb, Sb, Bi, and Ce on Microstructure of Heavy-Section Nodular Iron Castings," *AFS Transactions*, vol 79, p 247 (1971).
14. S. I. Karsay; *Production of Ductile Cast Iron I*, p 41 (1976).
15. C. W. Thomas; "The Effect of Antimony on the Structure of Low-Magnesium Hypereutectic Irons Containing Proportions of Nodular Graphite," *BCIRA Journal*, vol 30, Report No. 1453, p 36 (Jan 1982).
16. E. Campomanes; "The Suppression of Graphite Deterioration in Heavy Ductile Iron Castings," *Giesserei*, vol 65 Nr. 20, p 535 (1978).
17. S. Morita et al; "Influence of Si on the Formation of Spheroidal Graphite Cast Iron," *Journal of the Iron and Steel Institute of Japan*, vol 42, No.3, p 309 (1956).
18. R. W. Reesman and C. R. Loper, Jr.; "Heavy-Section Ductile Iron as Affected by Certain Processing Variables," *AFS Transactions*, vol 75, p 1 (1967).
19. N. L. Church and R. D. Schelleng; "Detrimental Effect of Calcium on Graphite Structure in Heavy-Section Ductile Iron," *AFS Transactions*, vol 78, p 5 (1970).
20. S. I. Karsay and E. Campomanes; "Control of Graphite Structure in Heavy Ductile Iron Castings," *AFS Transactions*, vol 78, p 85 (1970).
21. N. L. Church and R. D. Schelleng, *AFS Transactions*, vol 78, p 465 (1970).
22. S. Okada and Y. Maebashi; "The Mechanical Properties and Structures of Heavy Ductile Iron Castings," *Journal of the Japan Foundrymen's Society*, vol 43, No 3, p 13 (1971).
23. R. Barton; "Nodular Iron: Possible Structural Defects and Their Prevention," *Foundry Trade Journal*, vol 155, No. 3267, p 40 (July 14, 1983).
24. T. C. Xi et al; "The Formation and Prevention of Chunky Graphite in Slowly Solidified Non-Alloy Spheroidal Irons," *Fonderie Found d'aujourd'hui*, Nr. 46, S 14 (1985).
25. N. Yingyi and Z. Zhu; "A Study of the Rare Earth Effect on Chunky Graphite Formation in Heavy-Section Ductile Iron," *The Foundryman*, 390 (Aug 1988).
26. R. Helms and J. Ziebs; Seminar "Container for Radioactive Materials Made from Nodular Cast Iron," in Berlin, p 67 (June 9–10, 1987).
27. D. Aurich, R. Helms, and K. E. Wieser; Seminar "Container for Radioactive Materials made from Nodular Cast Iron," in Berlin, p 121 (June 9–10, 1987).
28. QA Committee (JAPAN); Seminar "Container for Radioactive Materials Made from Nodular Cast Iron," in Berlin, p 267 (June 9–10, 1987).
29. K. B. Palmer; "Effect of Cast Section Size on Fatigue Properties and the Prevention of Corrosion Fatigue of Nodular Irons," *The British Foundryman*, vol 75, p 201 (Nov 1982).
30. T. Shiota and S. Komatsu; "Influence of Graphite Nodule Diameter on Fatigue Strength and Crack Propagation Behavior of Ferritic Spheroidal Graphite Cast Irons under Rotational Bending," *IMONO*, vol 54, No. 7, p 14 (1982).
31. A. G. Fuller; "Effect of Graphite Form on Fatigue Properties of Pearlitic Ductile Irons," *AFS Transactions*, vol 85, p 527 (1977).
32. K. Kuribayashi et al; "Elastic-Plastic Fracture Toughness in Nodular Cast Iron," *ISIJ*, vol 69, No.6, p 663 (1983).
33. P. Bhandhubanyong; Paper for PhD degree, Tokyo University (19
34. J. M. Motz; Seminar "Containers for Radioactive Materials Made from Nodular Cast iron" in Berlin, p 199 (June 9–10, 1987).
35. S. I. Karsay; *Production of Ductile Cast Iron I*, p 113 (1976).